RSC Advances

Cite this: *RSC Advances*, 2012, **2**, 12378–12383

www.rsc.org/advances

PAPER

Singlet oxygen photogeneration and 2,4,6-TCP photodegradation at Pt/TiO_2 under visible light illumination†

Xuefeng Hu,*[a] Huanhuan Ji[ab] and Lei Wu[ab]

Received 1st August 2012, Accepted 18th October 2012
DOI: 10.1039/c2ra21661b

Pure and Pt nanoparticle-modified rutile TiO_2 were synthesized *via* hydrolysis of $TiCl_4$ in the absence or presence of Pt nanoparticles. HRTEM, XRD, and SEM were used to characterize the structure of the prepared catalysts. The resulting modified TiO_2 catalysts show extended visible light absorbance. Photodegradation of 2,4,6-trichlorophenol (2,4,6-TCP) over these photocatalysts was investigated under visible light illumination. The Pt nanoparticles facilitate the separation of photogenerated electron–hole pairs at low Pt content, then enhances the photodegradation rate of 2,4,6-TCP. 0.18Pt–TiO_2 achieved the best photocatalytic activity among the tested catalysts. It was found that singlet oxygen rather than $^{\bullet}OH$ acts as the main oxidative species for the degradation of 2,4,6-TCP according to the experimental results. The degradation intermediates of 2,4,6-TCP were identified and the degradation pathway was proposed. Pt nanoparticles on TiO_2 significantly enhance O_2 adsorption and the formation of $^{\bullet}O_2^-$. The rutile surface is a favorable condition for stabilizing $^{\bullet}O_2^-$. These properties of the Pt nanoparticle-modified rutile TiO_2 facilitate the formation of $^1O_2$ *via* the reaction of superoxide anions with holes.

Introduction

Many nanomaterials are able to sensitize the formation of singlet oxygen ($^1O_2$) upon photoexcitation.[1] Photogeneration of $^1O_2$ is known to play important roles in the photooxidation of organic compounds and the photodynamic therapy treatment of cancer. $^1O_2$ photogeneration at a TiO_2 surface under UV light illumination has been reported.[2] However, the TiO_2 photocatalytic degradation of organic pollutants proceeds mainly from the exertions of $^{\bullet}OH$ produced by the oxidation of water and $^{\bullet}O_2^-$ produced by the reduction of oxygen in air.[3,4] The roles of $^1O_2$ were often ignored in the TiO_2 catalyzed organic pollutants photodegradation although $^1O_2$ has been reviewed as a strong oxidizing reagent for organic pollutant degradation.[5,6] The photodegradation of organic pollutants *via* the $^1O_2$ mechanism conventionally requires organic photosensitizers.[7,8] However, these organic photosensitizers are prone to photodegradation under photoillumination, which reduces the efficiency of the $^1O_2$ generation.[7–9] Janczyk *et al.* reported the surface modification of TiO_2 with F^- and silyl groups leading to the photodegradation of cyanuric acid.[10] $^1O_2$ was thought to be responsible for the first steps of cyanuric acid structure destruction. However, the photogeneration of the $^1O_2$ occurred only under UV light illumination because of the wide band gap of TiO_2 (3.0 eV for the rutile phase and 3.2 eV for the anatase phase), which limits its application range.

Considering mechanisms of photocatalytic oxidation at excited TiO_2, the formation of singlet oxygen on TiO_2 was proposed to occur *via* two possible pathways: electron transfer pathway or energy transfer pathway. Nosaka *et al.* proposed that the generation of $^1O_2$ is probably caused by an electron transfer process *via* two steps.[2] The first step is the reduction of O_2 to $^{\bullet}O_2^-$ by photogenerated conduction band electrons. The second step is the oxidation of $^{\bullet}O_2^-$ to $^1O_2$ by photogenerated holes. Janczyk *et al.* claimed that the $^1O_2$ formation is based on energy transfer instead of the electron transfer mechanism.[10] They explained this as a result of the surface modification of TiO_2 with F^- and silyl groups, which suppressed the interfacial electron transfer pathway and enhanced the energy transfer pathway. Many investigations have indicated that the noble metal (Ag, Au, Pt) in TiO_2/noble metal heterostructures can obviously promote an interfacial charge transfer process and also extend the light response to the visible region.[11] The noble metal modified TiO_2, used for organic pollutant photodegradation, usually exists in the anatase phase and the active species for the organic pollutant oxidation was $^{\bullet}OH$.[12,13]

Chlorinated phenols are used in the pesticide field as fungicides and disinfectants and are also important chemicals in a number of industrial processes. 2,4,6-TCP was used as a model pollutant because it is an anticipated human carcinogen and there are sufficient cases of carcinogenicity. In this study, Pt nanoparticle-modified rutile TiO_2 catalysts were prepared and

[a]*Key Laboratory of Coastal Zone Environmental Processes, Yantai Institute of Coastal Zone Research, Chinese Academy of Sciences, Yantai Shandong 264003, P. R. China. E-mail: xfhu@yic.ac.cn; Fax: +86-535-2109000; Tel: +86-535-2109157*
[b]*University of Chinese Academy of Sciences, Beijing 100049, PR China*
† Electronic Supplementary Information (ESI) available. See DOI: 10.1039/c2ra21661b

used for the photodegradation of 2,4,6-TCP under visible light illumination. In contrast to previous studies, the results indicate that $^1O_2$, rather than $^{\bullet}OH$, acts as the main oxidative species for the platinized rutile TiO_2 photocatalyzed degradation of 2,4,6-TCP. The Pt nanoparticle-modified TiO_2 sensitized formation of $^1O_2$ under visible light illumination shows its potential application in photodynamic therapy and the selective photooxidation of organic compounds (such as the peroxidation of olefins).

Materials and methods

Chemicals

Chloroplatinic acid hexahydrate (99.9%), sodium borohydride (98%), methanol (99.9%), 1,4-benzoquinone(99%), 2,6-dichloro-1,4-benzoquinone (>98%) and 2,2,6,6-tetramethyl piperidine were purchased from Acros Organics. Titanium tetrachloride ($TiCl_4$) was obtained from Shanghai Meixing Chemistry CO. Ltd., NaN_3 and 2,4,6-TCP were supplied by Aladdin Chemistry Co. Ltd. All reagents were used as received without further purification. Deionized water was used throughout this study.

Photocatalyst preparation

The synthesis of the Pt colloidal solution was performed by following the reported method with slight modification.[14] 2.5 mL 0.02 M H_2PtCl_6 and 12.5 mL 0.4 M cetyltrimethylammonium bromide (CTAB) were mixed with 29.5 mL deionized water in a 100 mL round bottom flask at room temperature. The mixture was stirred at room temperature for 10 min and was heated to 50 °C for another 10 min. Then, 3 mL of 0.5 M ice-cooled $NaBH_4$ solution was added. The gas evolved inside the flask was released by inserting a needle through the septum. Pt colloidal solution solutions were obtained after a reaction time of 15 h. The Pt nanoparticle-modified TiO_2 was synthesized by hydrolysis of $TiCl_4$ in the Pt colloidal solution. The typical procedure was as follows: an amount of $TiCl_4$ was added to ice-cooled concentrated HCl, stirred for 30 min. The mixture was then dropped to the prepared Pt colloidal. After stirring for 1 h, the solution was heated to 75 °C for 12 h. After that, the products were cooled to room temperature and separated by centrifugation at 12 000 rpm for 10 min The products were then washed 5 times with hot distilled water. The final samples were dried at 80 °C and then collected. The actual Pt molar content on the prepared catalysts was 0.06%, 0.12%, 0.18%, 0.29%, 0.40% according to the ICP-MS data, and these catalysts were denoted as 0.06Pt–TiO_2, 0.12Pt–TiO_2, 0.18Pt–TiO_2, 0.29Pt–TiO_2 and 0.40Pt–TiO_2 accordingly. The pure TiO_2, synthesized using the same procedure but with deionized water instead of the Pt colloidal solution. All the prepared TiO_2 catalysts were then heated in a muffle furnace at 450 °C for 3 h.

Measurements and analysis

X-ray diffraction (XRD) measurements were performed on a Shimadzu XRD-6100 diffractometer with Cu-Kα radiation (1.5406 Å). X-ray photoelectron spectroscopy (XPS) was conducted on a Perkin–Elmer PHI 5000C ESCA system to determine the surface electronic states of the catalysts. All the binding energy values were calibrated using C 1s = 284.8 eV as a reference. The Pt molar content of the catalysts were detected using a Perkin Elmer ICP-MS (ELAN DRC II) after digestion. A high-resolution transmission electron microscope (HRTEM) image was obtained on a JEOL JEM-2100 at 200 KV. The electron spin resonance (ESR) signals of the singlet oxygen ($^1O_2$) trapped by 2,2,6,6-tetramethyl piperidine (TEMP) were detected at ambient temperature on a Bruker (ESP 300E) spectrometer. The catalyst was excited with a Nd:YAG laser at 532 nm and 355 nm. Scanning electron microscopy characterizations of the catalysts were performed with a Hitachi S4800 instrument. A Hitachi U-3100 was used to record the UV-VIS diffuse reflectance absorption spectra of the catalysts. UV-VIS absorption spectra of the solution were measured on a Beckman DU-800 UV spectrometer. The photodegradation of 2,4,6-TCP was analyzed by Waters 2695e high performance liquid chromatography (HPLC) with a SunFire C18 5 μm column. HPLC-MS (Thermo Fisher Scientific, LCQ Fleet ion trap spectrometer) was used to identify the degradation intermediates. Changes in total organic carbon (TOC) were determined using a total organic carbon analyzer (Shimadzu TOC 5000).

Photocatalytic reactions

The light source used in this study was a 300 W Xe lamp (CEL-HXUV300, Beijing Changtuo Lighting Corporation, China) equipped with a glass filter restricting the transmission of wavelength below 400 nm. The original spectrum of the lamp is shown in Fig. S1, ESI.† In a typical photocatalytic reaction, 30 mg catalyst was dispersed in 30 mL aqueous solution of 10^{-4} M 2,4,6-TCP. Prior to illumination, the suspension was magnetically stirred in the dark for 30 min to ensure the establishment of an adsorption/desorption equilibrium. At a given time, the reaction suspension samples were collected, centrifuged, and then filtered to remove the catalyst. The filtrates were analyzed with HPLC, TOC and UV-VIS absorption spectra.

Results and discussion

Characterization of the prepared photocatalyst

Fig. 1 shows the XRD patterns of the as-prepared TiO_2 and 0.18Pt–TiO_2 samples. These patterns can be well indexed to tetragonal rutile (JCPDS No. 21-1276). No peaks of anatase or brookite phases are detected, indicating the high purity of the rutile TiO_2. It was reported that the XRD diffractions of cubic phase platinum locate at about 39.8°, 46.3°, 67.5°, and 81.3° (JCPDS No. 04-0802), which would not overlap with the diffractions of rutile TiO_2 and would be easily detected. However, no diffraction peak of crystalline Pt was observed at this low concentration, showing good agreement with the previous studies.[15,16] The particle size calculated from the diffraction peak of (110) are 19.2 nm for TiO_2 and 13.9 nm for 0.18Pt–TiO_2. The Pt nanoparticles significantly decreased the crystallite size of the catalyst, which is also observed in the literature.[15] The existence of Pt nanoparticles during TiO_2 preparation does not affect the XRD pattern of TiO_2. However, the diffraction peak of TiO_2 (101) broadened and shifted to high angle in the presence of Pt nanoparticles. According to Bragg's law, $n\lambda = 2d\sin\theta$, the lower the value of θ, the larger the spacing. So, we can conclude that the presence of Pt decreased the value of the d-spacing. XPS was used to

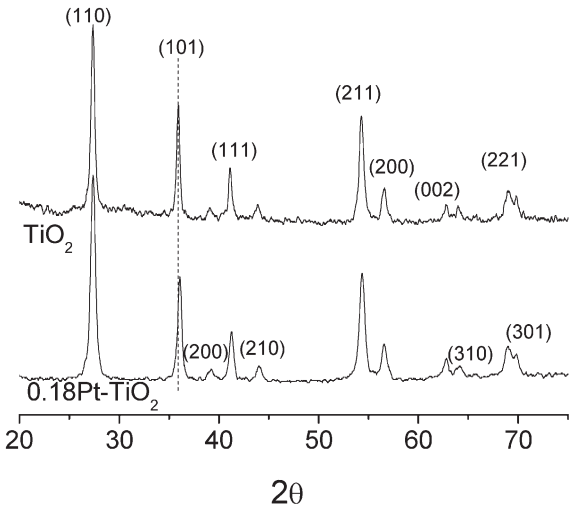

Fig. 1 XRD patterns of the prepared TiO_2 and 0.18 mol% Pt modified TiO_2 (0.18Pt–TiO_2).

investigate the chemical status of Pt in the prepared Pt/TiO_2 catalyst. The broad Pt (4f)-spectrum (Fig. S2, ESI†) may tentatively be deconvoluted into three components: Pt^0 ($4f_{7/2}$) at a binding energy of 70.8, PtO ($4f_{7/2}$) and PtO_2 ($4f_{7/2}$) at binding energies of 73.0 and 75.0 respectively. It is reported that the heat treatment of Pt nanoparticles supported on oxides (such as TiO_2, SiO_2, CeO_2) results in the formation of oxidized Pt species, which show higher binding energies and indicate strong interactions between the Pt and oxides.[17,18] The modified catalyst showed an increase of absorption over the entire visible region after Pt nanoparticle modification (Fig. S3, ESI†). Similar absorption spectra for Pt–TiO_2 were obtained and discussed in other work.[19,20] Belloni *et al.* reported that the absorption properties of platinized TiO_2 depend on the optical properties of the metal, the matrix and the volume fraction of the metal in the nanocomposite.[19] In their work, the absorption in the visible region of Pt–TiO_2, with 1% Pt, reached more than 30% of the intensity at the maximum. The absorption of 0.18Pt–TiO_2 in the visible region was *ca.* 10% of the intensity at the maximum in our study.

Fig. 2A shows the SEM images of the 0.18Pt–TiO_2 sample. A lot of short nanorods were observed in the sample, which is similar to the pure rutile TiO_2 (not shown). These nanorods were of 30–60 nm in diameter and less than 350 nm in length. The size and morphology of the sample were further analyzed by HRTEM. Pt nanoparticles were embedded in the TiO_2 matrix, as shown in Fig. 2B. The Pt nanoparticles with sizes between 5 nm to 30 nm exhibited an uneven dispersion. The average size of 20 Pt nanoparticles in the TEM image was calculated to be 11 nm. Fig. 2C reveals the local crystal structure of the boundary between TiO_2 and a Pt particle (the circle part at Fig. 2B). The TiO_2 crystal lattice have a *d*-spacing of 0.32 nm, attributed to the (110) plane of the rutile-type TiO_2 crystals. In the Pt particles, lattice fringes with a *d*-spacing of 0.22 nm are observed, which correspond to the (111) spacing of a f.c.c. Pt structure (JCPDS No. 65-2868). The distinguished interface and the continuity of the lattice fringes between the TiO_2 and Pt nanoparticles confirms their strong interaction.[21] It has been reported that

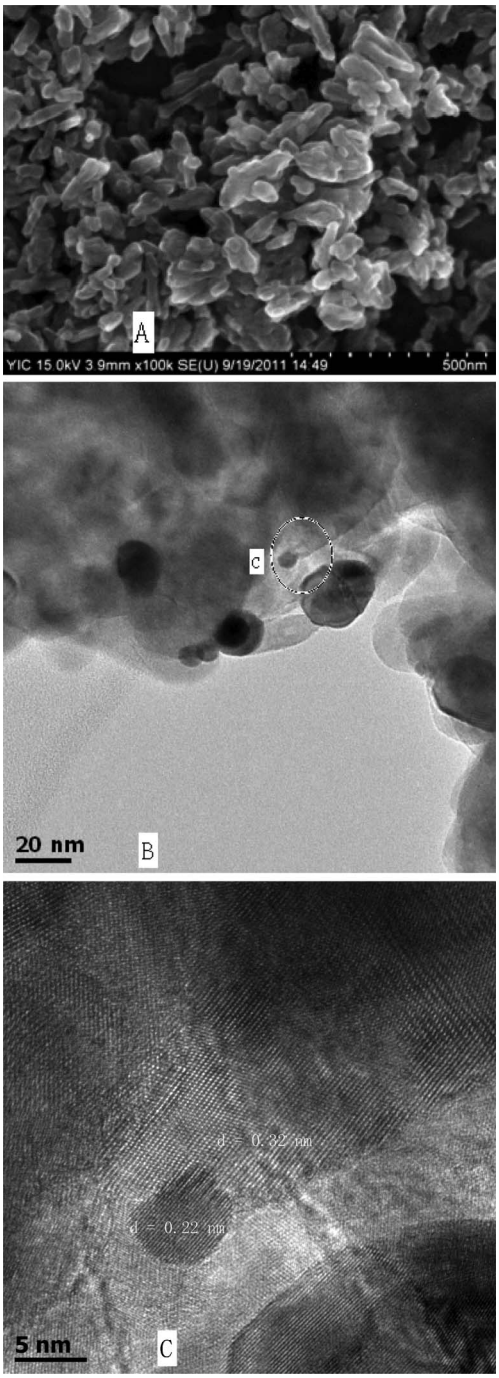

Fig. 2 A) SEM of 0.18Pt–TiO_2. B) TEM of 0.18Pt–TiO_2. C) HRTEM of the circle part at B.

the (110) facets of rutile TiO_2 are prone to collect electrons,[22] which greatly facilitates the transfer of electrons from the TiO_2 to the Pt nanoparticles, and enhances the separation of holes and electrons.

Photocatalytic activity for the degradation of 2,4,6-TCP

Fig. 3A compares the kinetics of the photodegradation of 2,4,6-TCP under visible illumination in the presence of different catalysts. Negligible reaction was observed in the presence of pure rutile TiO_2. Upon modification with Pt nanoparticles, the

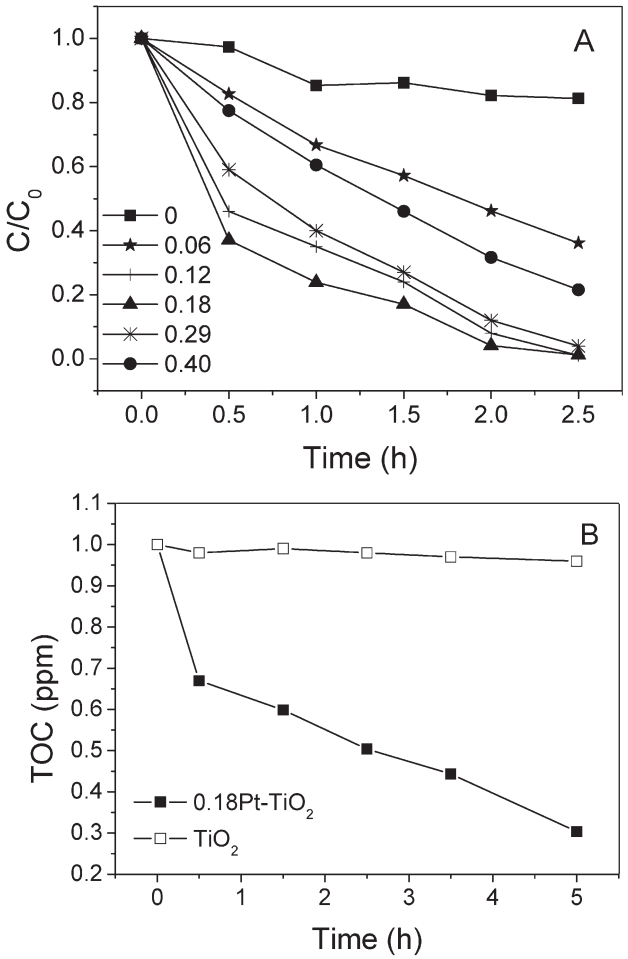

Fig. 3 A) Photodegradation of 2,4,6-TCP in the presence of different Pt content catalysts. B) TOC removal of 2,4,6-TCP in the presence of 0.18Pt–TiO_2 and pure TiO_2 under visible light irradiation.

degradation rate of 2,4,6-TCP was markedly enhanced. It can be found that the degradation rate of 2,4,6-TCP is increased with increasing of the Pt content when it was below 0.18 mol%, and decreased with the increase of the Pt content when it was higher than 0.18 mol%. The rutile structure of TiO_2 is known for the low photodegradation activity of organic species in aqueous solutions. This feature may be related to its ineffective oxygen reduction and efficient electron–hole pair recombination.[23] For the Pt modified catalysts, photogenerated electrons are transferred from the rutile TiO_2 conduction band to the Pt nanoparticles and the holes accumulate in the TiO_2 valence band. O_2 can be reduced by electrons at the Pt nanoparticles to $^{\bullet}O_2^-$, and in turn the reactive oxygen species form in the aqueous suspension.[24,25] However, the Pt nanoparticle is itself an electron–hole recombination center.[26] Thus, at high Pt nanoparticle concentration the increased electron–hole recombination rate on Pt has a larger deleterious effect than the increased oxygen reduction on Pt, which enhances photoactivity. This results in an optimum content of Pt being ~0.18 mol%, where a higher content of Pt was detrimental to the enhancement of the photoactivity. Total organic carbon (TOC) experiments were performed to evaluate the mineralization ratio of 2,4,6-TCP in the presence of the 0.18Pt–TiO_2 catalyst. The removal of TOC of 2,4,6-TCP was about 50% after 2.5 h illumination, and the TOC continued to decline afterwards, as observed in Fig. 3B. This means that 2,4,6-TCP and its organic degradation intermediates can be oxidized to harmless CO_2, H_2O and inorganic ions in this reaction system.

The reaction solution was initially colorless, but it turned pink and decayed finally as the oxidation proceed in the presence of Pt nanoparticle-modified rutile TiO_2. In the previously proposed mechanism for the TiO_2-mediated photodegradation of aromatic organic pollutants, $^{\bullet}OH$ was thought to be the main oxidative species for the degradation. Hydroquinones or catechols were the initial and main products formed by $^{\bullet}OH$ attack on the *para* or *ortho* positions of the aromatic ring.[27,28] These intermediates, produced from $^{\bullet}OH$ attack, do not display a pink color in aqueous solution. The formation of a pink colored intermediate indicates that another oxidative species different from $^{\bullet}OH$ is responsible for the photodegradation of 2,4,6-TCP.

Identification of the oxidative species and degradation intermediates

To study the main oxidative species for the degradation of 2,4,6-TCP, different oxidative species scavengers were added to the catalytic system, as shown in Fig. 4. The photodegradation of 2,4,6-TCP showed an insignificant decrease when ethanol, the $^{\bullet}OH$ scavenger, was added in the presence of 0.18Pt–TiO_2. This indicates that $^{\bullet}OH$ is not the main oxidative species for the degradation of 2,4,6–TCP. It was observed that the addition of benzoquinone (BQ, a very efficient scavenger of $^{\bullet}O_2^-$) and Na_2EDTA (a hole scavenger) both hindered the degradation of 2,4,6-TCP almost completely. The existence of a hole or electron scavenger would suppress their recombination and increase the lifetime of the separated electron and hole. The photodegadation should not be inhibited completely when BQ or Na_2EDTA are added, if hole or $^{\bullet}O_2^-$ act as the main oxidative species. This means that $^{\bullet}O_2^-$ and the hole are involved in the formation of the reactive oxidative species, but they are not the direct oxidant for 2,4,6-TCP degradation. It was also observed that the degradation was inhibited by the addition of NaN_3, an efficient quencher for $^{\bullet}OH$ and $^1O_2$. Rate constants for the hydroxyl radical and the singlet oxygen scavenging by NaN_3 are 7.5×10^9

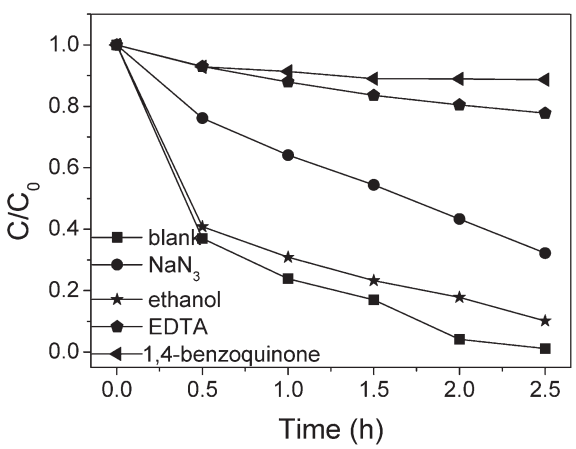

Fig. 4 0.18Pt–TiO_2 photocatalyzed degradation of 2,4,6-TCP in the presence of scavengers.

and 5 × 10^8 M^{-1} s^{-1},[10] respectively. For comparison, in the case of ethanol these numbers are 1.5 × 10^9 and *ca.* 10^3 M^{-1} s^{-1},[10] respectively. The different effects of added NaN_3 and ethanol on 2,4,6-TCP degradation indicated that $^1O_2$ should be the main oxidative species.

The oxidation of chlorophenols by $^1O_2$ was reported to result in the formation of hydroperoxides that dehydrated to form *p*-benzoquinone derivatives.[29] The *p*-benzoquinone derivative of the photooxidation of 2,4,6-TCP should be 2,6-dichloro-1,4-benzoquinon (DCQ). The aqueous photoreaction of DCQ produced 2,6-dichlorohydroquinone and 2,6-dichloro-3-hydroxy-1,4-benzoquinone (DCHB) as reported earlier.[30] DCQ, DCHQ and DCHB intermediates were observed in our experiments. 2,6-Dichloro-1,4-benzoquinon (DCQ) was identified by HPLC after comparison with authentic sample. 2,6-dichlorohydroquinone (DCHQ) and 2,6-dichloro-3-hydroxy-1,4-benzoquinone (DCHB) were identified by high performance liquid chromatography mass spectrometry (HPLC-MS) (Fig. S4, ESI†). UV-VIS absorbance at 524 nm, the source of the pink color, was observed during the photoreaction due to the formation of DCHB (Fig. S5, ESI†). It is reasonable to assume that the oxidation of 2,4,6-TCP by $^1O_2$ in this way, Fig. 5. It was previously demonstrated that $^{\bullet}N_3$ was generated during the quenching of $^1O_2$ by NaN_3.[31] $^{\bullet}N_3$ is a rather active oxidant that can react with 2,4,6-TCP, which lead to the photodegradation reaction of 2,4,6-TCP not being completely inhibited in the presence of NaN_3.

We have further employed an ESR technique to detect the photogeneration of $^1O_2$ by Pt–TiO_2 using 2,2,6,6-tetramethyl piperidine (TEMP) as the spin trap under 355 nm and 532 nm laser illumination. As shown in Fig. 6A and 6B, the characteristic ESR spectra, containing three equal-intensity lines from nitroxide radical (TEMPO), were successful determined during UV and visible illumination, and the signal intensity increased with the illumination time. The intensity of ESR signals illuminated at 355 nm is stronger than that illuminated at 532 nm after the same illumination time. This can be attributed to the strong absorbance of the catalyst at 355 nm that enhanced the formation of excited electrons, and then the formation of $^1O_2$. Control experiments showed that the nitrooxide radical signal can not be observed in the presence of NaN_3 after illumination at 355 nm for 180 s (Fig. S6, ESI†).

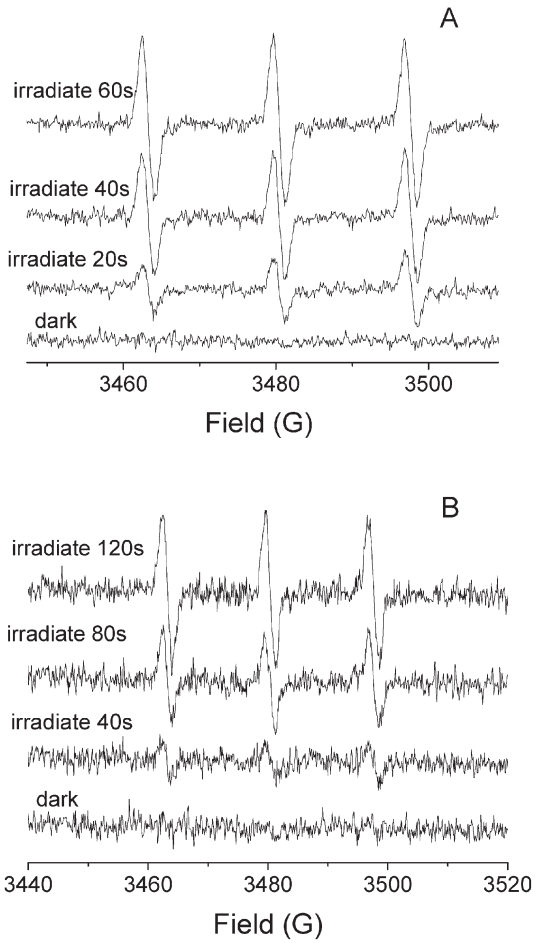

Fig. 6 ESR spectra of TEMP-$^1O_2$ adducts in aqueous solution. A) 0.18Pt–TiO_2 illuminated with 355 nm laser; B) 0.18Pt–TiO_2 illuminated with 532 nm laser.

Mechanism of singlet oxygen photogeneration

Hwang *et al.* reported recently that $^1O_2$ can be formed through direct sensitization by PVP dispersed Pt nanoparticles.[32] The formation of $^1O_2$ on Pt/TiO_2 was proposed to take place *via* the following possible mechanisms: 1) direct sensitization of Pt nanoparticles; 2) energy transfer as a result of electron–hole

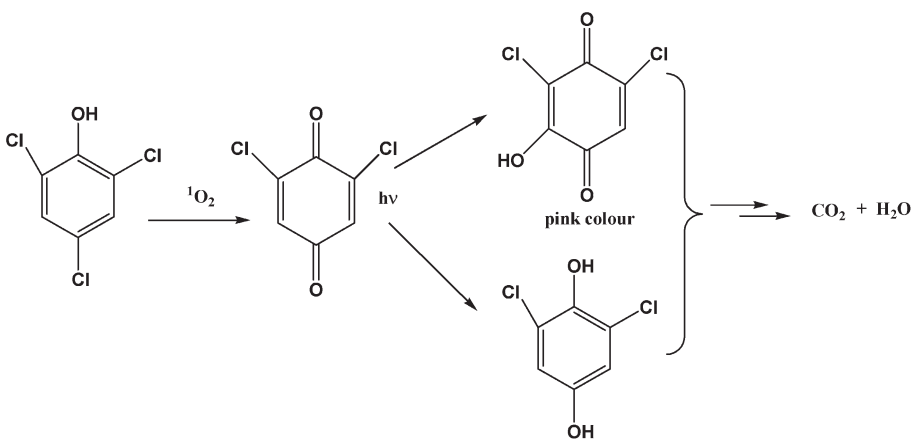

Fig. 5 Oxidation pathway of 2,4,6-TCP by $^1O_2$.

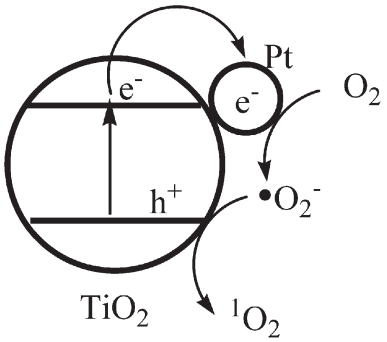

Fig. 7 Formation mechanism of $^1O_2$ on Pt nanoparticles modified rutile TiO_2.

recombination; and 3) electron transfer process, reaction of superoxide anion with hole. The hole and $^{\bullet}O_2^-$ scavenger would not affect the formation of $^1O_2$ if it was generated by the sensitization of Pt nanoparticles embedded on TiO_2. CTAB dispersed Pt nanoparticles in aqueous solution (1 g L^{-1}) cannot catalyze the degradation of 2,4,6-TCP under photoexcitation in this research. So, the photodegradation of 2,4,6-TCP can not be explained by the direct photosensitization of Pt nanoparticles. It has been reported that Pt nanoparticles on TiO_2 significantly enhance O_2 adsorption and the formation of $^{\bullet}O_2^-$.[26] The rutile surface is a favorable condition to stabilize $^{\bullet}O_2^-$.[33] These properties of Pt nanoparticle-modified TiO_2 facilitate the formation of $^1O_2$ *via* reaction of superoxide anions with holes, Fig. 7.

The present work demonstrates the photogeneration of $^1O_2$ and photodegradation of 2,4,6-TCP in the presence of Pt nanoparticle-modified rutile TiO_2 under visible illumination. The Pt nanoparticles contribute to separating distinctly the charges of electrons and holes generated in TiO_2 by visible illumination. O_2 can be reduced by the conduction band electron to $\cdot O_2^-$, which is oxidized by a hole to $^1O_2$. The formed $^1O_2$ is then involved in the primary oxidation reaction of 2,4,6-TCP. The presented results may shine some light on the mechanism of $^1O_2$ generation at the modified rutile TiO_2 surface and chlorophenols oxidation. On the other hand, the visible photogeneration of $^1O_2$ by the catalyst shows its potential application in photodynamic therapy and photooxidation of organic compounds.

Acknowledgements

The generous supports by the National Natural Science Foundation of China (No. 41076040, No. 20807036), the Chinese Academy of Sciences (KZCX2-YW-JS208) and the Yantai Science & Technology Bureau (Project 2010160) are acknowledged.

References

1 S. Z. Wang, R. M. Gao, F. M. Zhou and M. Selke, *J. Mater. Chem.*, 2004, **14**, 487–493.
2 Y. Nosaka, T. Daimon, A. Y. Nosaka and Y. Murakami, *Phys. Chem. Chem. Phys.*, 2004, **6**, 2917–2918.
3 M. R. Hoffmann, S. T. Martin, W. Choi and D. W. Bahnemann, *Chem. Rev.*, 1995, **95**, 69–96.
4 C. C. Chen, W. H. Ma and J. C. Zhao, *Chem. Soc. Rev.*, 2010, **39**, 4206–4219.
5 M. C. DeRosa and R. J. Crutchley, *Coord. Chem. Rev.*, 2002, **233–234**, 351–371.
6 A. H. Dwivedi and U. C. Pande, *Sci. Revs. Chem. Commun.*, 2012, **2**, 41–65.
7 X. Z. Li, W. Zhao and J. C. Zhao, *Sci. China, Ser. B: Chem.*, 2002, **45**, 421–425.
8 M. Stylidi, D. I. Kondarides and X. E. Verykios, *Appl. Catal., B*, 2004, **47**, 189–201.
9 T. Nyokong, *Coord. Chem. Rev.*, 2007, **251**, 1707–1722.
10 A. Janczyk, E. Krakowska, G. Stochel and W. Macyk, *J. Am. Chem. Soc.*, 2006, **128**, 15574–15575.
11 X. B. Chen and S. S. Mao, *Chem. Rev.*, 2007, **107**, 2891–2959.
12 H. Haick and Y. Paz, *J. Phys. Chem. B*, 2003, **107**, 2319–2326.
13 C. Quinones, J. Ayala and W. Vallejo, *Appl. Surf. Sci.*, 2010, **257**, 367–371.
14 S. H. Joo, J. Y. Park, C. K. Tsung, Y. Yamada, P. D. Yang and G. A. Somorjai, *Nat. Mater.*, 2008, **8**, 126–131.
15 M. Moonsiri, P. Rangsunvigit, S. Chavadej and E. Gulari, *Chem. Eng. J.*, 2004, **97**, 241–248.
16 C. B. Zhang, H. He and K. Tanaka, *Catal. Commun.*, 2005, **6**, 211–214.
17 J. R. Croy, S. Mostafa, J. Liu, Y. Sohn, H. Heinrich and B. R. Cuenya, *Catal. Lett.*, 2007, **119**, 209–216.
18 U. K. Kirner, K. D. Schierbaum and W. Göpel, *Fresenius' J. Anal. Chem.*, 1991, **341**, 416–420.
19 E. Kowalska, H. Remita, C. Colbeau, J. Hupka and J. Belloni, *J. Phys. Chem. C*, 2008, **112**, 1124–1131.
20 M. D. Driessen and V. H. Grassian, *J. Phys. Chem. B*, 1998, **102**, 1418.
21 J. K. Lim, S. A. Majetich and R. D. Tilton, *Langmuir*, 2009, **25**, 13384–13393.
22 E. Bae and T. Ohno, *Appl. Catal., B*, 2009, **91**, 634–639.
23 T. Ohno, K. Sarukawa and M. Matsumura, *J. Phys. Chem. B*, 2001, **105**, 2417–2420.
24 C. S. Turchi and D. F. Ollis, *J. Catal.*, 1990, **122**, 178–192.
25 L. Davydov and P. G. Smirniotis, *J. Catal.*, 2000, **191**, 105–115.
26 C. L. Muhich, Y. Zhou, A. M. Holder, A. W. Weimer and C. B. Musgrave, *J. Phys. Chem. C*, 2012, **116**, 10138–10149.
27 Y. Hou, X. Y. Li, Q. D. Zhao, X. Quan and G. H. Chen, *Environ. Sci. Technol.*, 2010, **44**, 5098–5103.
28 D. Zhao, C. C. Chen, Y. F. Wang, H. W. Ji, W. H. Ma, L. Zang and J. C. Zhao, *J. Phys. Chem. C*, 2008, **112**, 5993–6001.
29 K. Ozoemena, N. Kuznetsova and T. Nyokong, *J. Mol. Catal. A: Chem.*, 2001, **176**, 29–40.
30 G. Lente and J. H. Espenson, *J. Photochem. Photobiol., A*, 2004, **163**, 249–258.
31 J. R. Harbour and S. L. Issler, *J. Am. Chem. Soc.*, 1982, **104**, 903–905.
32 R. Vankayala, A. Sagadevan, P. Vijayaraghavan, C. L. Kuo and K. C. Hwang, *Angew. Chem., Int. Ed.*, 2011, **50**, 10640–10644.
33 T. Hirakawa, K. Yawata and Y. Nosaka, *Appl. Catal., A*, 2007, **325**, 105–111.